LA-UR -86-3221

CONF-8609135--4

Los Alamos National Laboratory is operated by the University of California for the United States Department of Energy under contract W-7405-ENG-36

LA-UR--86-3221

DE87 000152

TITLE: SOME EFFECTS ON THE KINETICS OF MUON-CATALYZED FUSION

AUTHOR(S): James S. Cohen

SUBMITTED TO: Proceedings of the International Symposium on Muon-Catalyzed Fusion
Tokyo, Japan
September 1-3, 1986

DISCLAIMER

Los Alamos Los Alamos National Laboratory
Los Alamos, New Mexico 87545

FORM NO 836 R4
ST NO 2629 5/81

SOME EFFECTS ON THE KINETICS OF MUON-CATALYZED FUSION

James S. Cohen
Theoretical Division
Los Alamos National Laboratory
Los Alamos, New Mexico 87545
U.S.A.

ABSTRACT

Two important stages in the kinetics of muon-catalyzed d-t fusion are discussed: (1) atomic thermalization and hyperfine-state relaxation preceding molecular formation and (2) muon stripping and X-ray production if sticking occurs after nuclear fusion. Thermalization is accurately treated by Monte Carlo simulation. It is shown that thermalization and triplet quenching of the $\alpha\mu$ atom may not finish before $dt\mu$ formation in low-tritium targets, but that epithermal transients are most important in high-tritium targets. A complete kinetic treatment of muon stripping from $\alpha\mu$ is made using newly calculated stripping (ionization and charge transfer) and inelastic excitation cross sections and explicitly treating the 2s-2p Stark mixing. The calculated values of the sticking probability and Kα $\alpha\mu$ X-rays per fusion are ω_s = 0.53% (0.59%) and $I_{K\alpha}/\chi$ = 0.23% (0.28%) at density ϕ = 1.2 (0.1) times liquid-hydrogen density. Sensitivities to the various kinetic rates are evaluated, and error bars are estimated.

I. INTRODUCTION

Discoveries in recent years, both experimental and theoretical, have demonstrated that the kinetics of muon-catalyzed fusion (MCF) is more complex than originally conceived.[1,2] In particular, experiments have observed transient rates in molecular formation (mf) of $dt\mu$ as well as density effects on $dt\mu$ formation and muon loss ("sticking"). Two explanations of the transient mf rates have been advanced: (1) quenching of the hyperfine (triplet) state of the $t\mu$ atom[2a] and (2) epithermal distributions of $t\mu$ atoms.[3,4] The mf rate depends strongly on both the hyperfine-spin state[5] and the velocity[3] of $t\mu$. New theoretical results for the time-dependent velocity and hyperfine-state distributions are presented in Sec. II. The (nonlinear) density dependence of the mf rate, discussed in the preceding talk by Leon[6], is not a subject of this talk. The present paper addresses the density dependence of the sticking probability. Two possible explanations of the density dependence of muon loss have also been proposed: (1) a hypothetical "bottleneck" state in the relaxation of $(dt\mu)^{**}$, which is formed in a state having a relatively low fusion rate[7], and (2) stripping of the μ^- from excited states of $\alpha\mu$ after muon sticking to the fusion α particle. New calculations of cross sections relevant to the latter are presented in Sec. III. These cross sections are used in Sec. IV in a "complete" kinetic treatment of the stripping process. The K-series $\alpha\mu$ X-rays per fusion as well as the muon reactivation probability are presented. The sensitivities of these quantities to the various rates are evaluated; of particular interest, it is shown that explicit treatment of Stark mixing of the 2s and 2p states is needed.

II. THERMALIZATION OF HOT tμ ATOMS

Muonic tritium atoms can be formed in deuterium-tritium mixtures in two ways: by direct capture of a free muon

$$\mu^- + T \rightarrow e + t\mu \qquad (1a)$$

or by transfer from dμ

$$d\mu + t \rightarrow d + t\mu \quad . \qquad (1b)$$

In the former case the tμ is formed with a kinetic energy of ~1 eV.[8] In the latter case the tμ recoils with an initial kinetic energy of 19 eV if the dμ is in the ground state at the time of transfer; however, the energy will be less by a factor of $1/n^2$ if transfer occurs from an excited state.[9] In either case, the energy of tμ, from which mf occurs, may be less and may also depend on the target density. Fortunately the results of this work are found not to be too sensitive to the initial energy as long as it is large compared to kT. Upon formation the two hyperfine levels of tμ are expected to be populated about statistically, i.e.,

$$[t\mu(\uparrow\uparrow)] \,/\, [t\mu(\uparrow\downarrow)] \propto 3 \quad . \qquad (2)$$

Afterwards the triplet level efficiently relaxes by charge exchange

$$t\mu(\uparrow\uparrow) + t \rightarrow t + t\mu(\uparrow\downarrow) + 0.241 \text{ eV} \quad . \qquad (3)$$

Thermalization of the initially hot tμ atom occurs by elastic and rovibra-

tional excitation collisions with the target molecules D_2, DT, and T_2.

Though cross sections for these molecular targets have not been calculated, cross sections for the atom-ion collisions $t\mu$+d and $t\mu$+t have been calculated. For $t\mu$+d collisions the hyperfine state of $t\mu$ is of little importance, but for $t\mu$+t the hyperfine splitting and spin coupling must be taken into account. In some cases, this has been done explicitly, but for others the effects of spin coupling have to be imposed on the results of symmetric charge-exchange calculations.[10] The various partial-wave atomic cross sections, calculated by Ponomarev and coworkers, were fit over the relevant energy range using modified effective-range expansions.[11] The integrated elastic and hyperfine-transition cross sections are shown in Fig. 1. Most notable is the very large size of the $t\mu$+d elastic cross section compared with the $t\mu$+t cross sections. The singlet (ground-state) $t\mu$+t cross section is very small at near-thermal energies.

Of course, thermalization calculations require the differential cross sections that are computed from the partial-wave results (only s and p waves are important at E<10 eV). The atomic cross sections are converted to molecular cross sections using the Sachs and Teller mass-tensor method.[12] In their method the actual molecular target is replaced by a hypothetical mass point that moves with the velocity of the target atom but has a tensor mass that depends on the structure of the molecule. The molecular cross sections are generally larger than the corresponding atomic cross sections.

The $t\mu$ kinetic energy distribution F(E,T) is described by the time-dependent Boltzmann equation. This equation is accurately solved by Monte Carlo simulation for given target temperature T and tritium fraction c_t. The initial energy distribution is taken to be Maxwellian with average energy E_0=1 eV. The details of the method will be given elsewhere;[11] 20 000 test atoms

were followed for each target condition, and the energies at selected times were placed in 50 energy bins. It was found that the energy distributions could usually be adequately fit by the sum of two Maxwellian functions, with temperature determined by a nonlinear least-squares fit. A typical Monte Carlo histogram and its fit are shown in Fig. 2.

The distribution functions are normalized to unity at all times. Of course, the number of $t\mu$ atoms is actually depleted by $dt\mu$ formation, but this process is not expected to affect seriously the velocity distribution (if the mf cross sections were known accurately, there would be no difficulty in including them explicitly). All the processes presently treated scale linearly with density, so it is sufficient to present the results at liquid-hydrogen density (LHD). Furthermore, the difference between the velocity distribution functions for the singlet and the triplet states is deemed negligible. The results of Monte Carlo simulation are as accurate as the cross sections used, and additional processes are easy to include once their rate is known. Of course, Monte Carlo is essentially a computer techniques.

The $t\mu$ kinetic-energy distribution (normalized to LHD) for several times after $t\mu(1s)$ formation are shown in Fig. 3 for a target consisting of 50% tritium at temperature 30 K. To put the times in perspective, the mf time under these conditions is ~6 ns (~1.5 units of reduced time on the graph). At this time the average $t\mu$ energy corresponds to a temperature over three times higher than the target temperature (the actual distribution is non-Maxwellian). Clearly it would be inappropriate to compare the experimental mf rate for such a target with the theoretical rate obtained by averaging the energy-dependent cross section over a Maxwellian at the target temperature. In Fig. 4 the average $t\mu$ energy is shown as a function of time for three different tritium fractions and two different temperatures; the higher c_t is,

the slower thermalization is. After 10 ns the c_t=0.9 target is still far from thermal equilibrium. However, a rather different picture emerges when the curves are placed on time scales relevant to MCF. The relevant time is then the mf time given by

$$\bar{t}_{mf} = (\phi\, c_d\, \lambda_{dt\mu})^{-1} \quad . \qquad (4)$$

Using the expansion

$$\lambda_{dt\mu} = c_d\, (\lambda^{(1)}_{dt\mu-d} + \lambda^{(2)}_{dt\mu-d}\, \phi) + c_t\, \lambda^{(1)}_{dt\mu-t} \qquad (5)$$

and the constants obtained experimentally by Jones et al.,[1b] we get the values of $\bar{t}_{mf}$ given in Table Ia for the target conditions used in Fig. 4 (ϕ=1). In Table Ib the corresponding average energies (expressed as effective temperature $E_{av}/1.5k$) obtained from the Monte Carlo simulations are given. Now it can be seen that at c_t=0.9 molecular formation is so slow that the $t\mu$ atoms still have time to thermalize even though the thermalization itself is also slow. On the other hand, at $c_t \lesssim 0.5$ where thermalization and mf are both much faster, the molecular formation wins the race. In the latter case the effective temperature of mf is not the target temperature. The theoretical energy-dependent mf rate must be averaged over the appropriate nonthermal energy distribution, and any distinctive resonant structure may be washed out.

The early-time transient mf rate contains a wealth of additional information. Arbitrarily defining the "epithermal period" to be the time before $E_{av}/1.5k$ falls below 600 K, we get the times given in Table II for ϕ=1. The transient lasts longest for high c_t. Since $\lambda_{dt\mu-t}$ is comparable in magnitude to $\lambda_{dt\mu-d}$ in the epithermal region,[3] unlike the thermal region where

$\lambda_{dt\mu-t}$ is relatively small, this transient effect is most important for high c_t. This is the condition in the S.I.N. experiment that saw a large transient effect.[2a] Knowing the mf rate and the energy distribution as a function of time, allows, at least in principle, one to obtain the mf rate constants at energies far higher than could be conveniently achieved under static laboratory conditions.

Finally in Fig. 5 the fractional triplet $t\mu$ population is shown. At t=0, a Boltzmann distribution is assumed; i.e., f_3=0.70 for E_o=1 eV. Triplet quenching occurs in the charge-exchange collision Eq. (3) and is rapid compared with mf at c_t=0.9 but slow compared with mf at c_t=0.1. The curves of Fig. 5 are for T=300 K, but the temperature dependence is weak.

We can summarize our observations on $t\mu$ kinetics as follows:

(1) Thermalization is mostly due to collisions with d except at very high c_t (c_t>0.9), but, of course, $dt\mu$ formation is all due to collisions with d. The upshot is that mf occurs before thermalization at low c_t.[i]

(2) Triplet quenching is due (almost) entirely to collisions with t. At low c_t, mf from the triplet state of $t\mu$ is important and hyperfine effects may be observable.

(3) Except at very early times, the energy distribution is insensitive to the initial conditions as long as E_o>>kT.

(4) Interpretation of the observed early-time (transient) behavior will require use of the nonequilibrium energy distributions and epithermal mf rates. Epithermal transients are most important at high c_t.

(5) Time-dependent nonthermal energy distributions may wash out the distinctive target-temperature dependence usually characterizing resonant

---

[i]This may not hold true at high densities after excited-state processes are included.

processes.

The present treatment of the $t\mu$ thermalization is by no means yet complete. One desirable improvement is inclusion of the effect of electronic structure on $t\mu$ scattering, $t\mu$+t in particular.[13] The greatest uncertainty attributable to this effect is at low temperature. Another possible improvement is inclusion of excited-state cross sections[9] (elastic, charge transfer, etc.). They may introduce a density dependence as well as additional dependence on the tritium fraction.

III. NEW CROSS SECTIONS FOR $\alpha\mu$ STRIPPING AND THE EFFECT OF TARGET STRUCTURE

When a muon sticks to the alpha particle after MCF, the $\alpha\mu$ recoils with a velocity of 5.84 a.u. The muon may be transferred or ionized in collisions with target D_2, DT, or T_2 molecules before it slows down to a velocity $\lesssim 1$, at which point it can be considered to be permanently lost as a fusion catalyst. All previous theoretical treatments have considered the collisions to occur with bare nuclei

$$\alpha\mu + d \rightarrow \begin{cases} \alpha + \mu + d & \text{(6a)} \\ \alpha + d\mu & \text{(6b)} \end{cases}$$

and have neglected the effect of different target masses. These approximations are probably justified since (1) the collision is (at least initially) fast and (2) $\alpha\mu$ is small compared to the electronic atom D or molecule D_2. However, in view of experimental evidence of a larger-than-predicted density dependence and a possible tritium-fraction dependence in the observed sticking probability ω_s,[1b] it was considered desirable to verify the

usual simplifications. Note that target structure can be expected to affect excited states $(\alpha\mu)_n$ more than the ground state $(\alpha\mu)_{1s}$, and such an effect would increase "ladder" ionization--i.e., successive excitation to higher states where stripping becomes more probable. The ladder effect certainly depends on density since collisional excitation completes directly with density-independent radiation. In addition to investigating possible target structure and mass effects, the new calculations were done to improve the accuracy of cross sections needed for muon reactivation calculations.

The classical-trajectory Monte Carlo (CTMC) method,[14] which has previously been shown to be reliable for calculating cross sections at velocities ~1 a.u., was used. The initial conditions of the atoms (muonic and electronic) are chosen from microcanonical distributions; this spherically symmetric distribution is appropriate as long as the ℓ-mixing collisions are relatively rapid. Hamilton's equations are then numerically integrated until the final state can be identified. Enough trajectories are run to reduce the statistical error of the stripping (ionization and charge transfer) cross section to 5%.

The CTMC method is applied in three ways: (1) collision of $\alpha\mu$ with a bare nucleus, p, d, or t, (2) collision of $\alpha\mu$ with an "atom" represented by a static effective potential (still a three-body calculation), and (3) collision of $\alpha\mu$ with an atom "de" in which the electron dynamics is also treated classically (a four-body calculation). The calculations of type 1 were done to determine the isotope effect as well as to establish a standard for comparison. In the calculations of type 2, the atom is represented with an r-dependent effective charge,[15] $(1+r)\exp(-2r)$, and will be denoted D_{eff}. This treatment shows the effect of electron shielding and has the advantage of utilizing the true (unperturbed) electron density. Calculations of type 3

were done to determine, in addition, the effect of direct collisions with the electron.

The three types of calculations for $\alpha\mu$+D were performed at velocities of 1 and 6 a.u. and $\alpha\mu$ levels n = 1, 2, and 3.[ii] The results, given in Table III, clearly show that the effect of the electron, whether treated statically or dynamically, is very small and certainly less than the uncertainty in the calculations. The results of calculation of type 1 for p, d, and t targets are given in Table IV at velocities of 2 and 6 a.u. The isotope effect is also found to be less than 5% at $v \gtrsim 2$. In conclusion, the cross sections for $\alpha\mu$+D or $\alpha\mu$+T are about the same as for $\alpha\mu$+d as long as $v \gtrsim 1$ a.u. The same must be true for $\alpha\mu+D_2$ (or DT or T_2), since the collision energy greatly exceeds the molecular binding energy. Hence using the same cross sections (as a function of velocity) for $\alpha\mu$ collisions with D_2, DT, and T_2 is justified.

IV. KINETICS OF MUON REACTIVATION AND X-RAY PRODUCTION

The initial sticking of a muon to the recoiling α particle after MCF depends only on the intramolecular dynamics and so is expected to be independent of target conditions. However, the observed sticking includes the effect of subsequent collisions that may strip the muon from the alpha particle. The processes important to muon stripping are shown in Fig. 6. The stripping itself occurs by either ionization, e.g. Eq. (6a), or charge transfer, e.g. Eq. (6b), and must take place before the $\alpha\mu$ is slowed from its initial velocity of 5.84 a.u. to a velocity less than about 1 a.u. Because

---

[ii] The same initial conditions are used in all three calculations so the relative precisions should be better than 5%.

both the slowing-down (stopping) and stripping rates depend linearly on density, no density dependence of the stripping probability can be obtained from the simplest possible description based on the competition between these two processes. The most likely source of a net density dependence would appear to be radiative processes,[16] which are independent of the density and important in $(q\mu)_n$ de-excitation at low n (n is the principal quantum number). The ionization and charge-transfer cross sections depend strongly on the state of $q\mu$. In addition to radiation, inelastic and Auger processes are important in establishing the distribution of n levels. These processes, in particular radiation, can also depend on ℓ. As shown in Fig. 6, it was found necessary to have separate populations only for the 2s and 2p states; i.e., Stark mixing can be assumed to be complete for $n \geq 3$. Processes which are assumed to be the same for 2s and 2p are shown in Fig. 6 with arrow heads pointing to the dashed line lying between the 2s and 2p levels. The stopping power is assumed to be independent of the $q\mu$ state and is taken to be the same as for protons at the same velocity (the mass dependence is quite weak at $v \geq 1$ a.u.). The possibility that the $q\mu$ ion may recombine with an electron may diminish the effective stopping power, especially at the lower velocities.

The stripping (including ionization and muon transfer) and excitation cross sections used are all new results calculated using the CTMC method (the same calculation gives all of them for a given initial n). As discussed in Sec. III it was found sufficient to neglect the effect of the target electronic structure and mass on these cross sections. The radiative rates were obtained by scaling the hydrogen-atom results given by Bethe and Salpeter.[17] The Auger and Stark rates were calculated using the formulas of Leon and Bethe.[18] The fits of the stopping power given by Anderson and Ziegler were used.[19] All these rates were included in the set of differential

equations describing the $\alpha\mu$ kinetics. In Figs. 7-10 some of the rates are shown for ϕ=1 as a function of v^2. In Fig. 7 the fractional energy loss per second (proportional to the stopping power divided by the velocity) is shown. The stripping and total excitation (summed over $n\geq 2$) rates for n=1 are also shown (the actual kinetics uses the state-to-state rates, not the sums). At the initial velocity the excitation cross section exceeds the stripping cross section, but this relation is reversed at lower velocities as charge transfer becomes more important. At any given time most of the $\alpha\mu$ atoms are in the ground state so these are the most important cross sections. In Fig. 8 rates affecting the population in n=2 are shown. By far the largest rate is the radiative rate. It is much larger than the Stark mixing rate so the 2s and 2p states will not be statistically populated (The 2p → 2s Stark transition rate is plotted). At most of the velocities of concern the rate for further excitation is substantially greater than the stripping rate. De-excitation other than by radiation is not important for n=2, but it is interesting to note that the inelastic de-excitation rate exceeds the Auger rate at v=6. In Fig. 9 the rates for n=3 are shown. For $n\geq 3$ the excitation rate exceeds all the de-excitation rates at the velocities of interest ($1\leq v\leq 6$ a.u.), so continued climbing of the ladder is most probable. The Stark mixing rate for n=3 still does not greatly exceed the radiative rate, but Stark mixing is not nearly so important for $n\geq 3$ since none of the substates have long radiative lifetime as does the 2s state. It will be shown later that most of the atoms that reach the n=3 level are stripped. The rates for n=6 are exhibited in Fig. 10. At n=6 the Auger de-excitation rate finally exceeds the inelastic de-excitation rate. Radiation is no longer of any importance.

The time-dependent state populations, stripping fraction R, and surviving fraction of the initial kinetic energy are shown in Fig. 11. The large

majority of the population is in the ground state at any given time, and the population in each higher level decreases monotonically with increasing n. The relative 2s and 2p populations are far from statistical. The actual ratio of 2s-to-2p populations depends in part on the ratio of their excitation cross sections from the ground state. The ratio assumed for this graph is $\sigma_{1,2p}/\sigma_{1,2s}=3$; the actual ratio probably exceeds this value at v~6 a.u. However, as will be shown later, the quantities of experimental interest are far less sensitive to this ratio.

The computer code describing the kinetics can include an arbitrary number of states. The stripping probability R, as well as the effective sticking probability $\omega_s=(1-R)\omega_s^o$,[111] are shown in Fig. 12 as a function of the number of $\alpha\mu$ levels included. Convergence is obtained with about 10 levels. The excited states of $\alpha\mu$ are responsible for increasing the stripping probability from ~0.3 to ~0.4. Even more important they are totally responsible for the density dependence of R.

The stripping results calculated in this paper assume the initial sticking distribution among $\alpha\mu$ states calculated by Hu.[20] This distribution is essentially the same as that calculated in other nonadiabatic calculations[21-22] as well as earlier in the adiabatic approximation.[16] It should be noted that all these calculations make the sudden approximation.[23] If the initial distribution were different the stripping probability would be changed. However, because the system of kinetic equations is linear, the results can be presented in a form allowing the sticking to be easily recalculated for any initial distribution. This is done in Table V, which

---

[111] Here and throughout this paper it is assumed that $\omega_s^o = 0.88\%$. If the true value is later found to be different, the results in the present paper for ω_s and I_K should be scaled accordingly.

gives the fraction of $\alpha\mu$ atoms starting in each state that is stripped.[iv] This tabulation also provides an interesting way for interpreting the kinetics. The stripping probability for an $\alpha\mu$ atom formed in the 2s state is appreciably greater than if it is formed in the 2p state. Otherwise, the higher the excitation, the greater the probability of stripping.

The results given so far have been for density ϕ=1. The stripping and effective sticking as a function of density for $0<\phi<1.4$ are shown in Fig. 13. The strongest dependence on ϕ occurs at low density. At extremely high densities where all collisional rates exceed all radiative rates, R approaches a constant. In the zero-density limit ω_s does <u>not</u> approach ω_s^o, but does become the same as the calculated value in Fig. 12 with n_{max}=1. Over the easily accessible range of densities, ϕ=0 to $\phi\simeq$1.4, R increases from ~0.3 to ~0.4. It is interesting to note that this variation is about the same seen as a function of n_{max} in Fig. 12; this similarity is not altogether coincidental.

Now we will turn to another aspect of $\alpha\mu$ kinetics that has been arousing a lot of experimental interest lately, namely, X-ray production. X-ray intensities contain additional information on the $\alpha\mu$ kinetics. They provide a useful test of muon-reactivation theories though, as we shall see, they are not <u>most</u> sensitive to the same rates. For convenience I will first define some notation that is needed. The average number of neutrons (i.e., the number of fusions) will be denoted χ. Then the average number of stickings over the active lifetime of a muon is given by $\omega_s^o\chi$. What is actually calculated in the present work is the average number of $\alpha\mu$ K-series X-rays per sticking, denoted $\gamma_{K\alpha}$ (or $\gamma_{K\beta}$, etc). The total average number of Kα X-rays per muon event is

---

[iv] This should not be confused with Fig. 12. In Table 5 ten levels are included in the calculation regardless of the initial state.

$$I_{K\alpha} = \gamma_{K\alpha}\, \omega_s^{\circ}\, \chi \quad .$$

but a more convenient quantity to compare with experiments is the number of Kα X-rays per fusion,

$$I_{K\alpha}/\chi = \gamma_{K\alpha}\omega_s^{\circ} \quad .$$

In this quantity the "uninteresting" density dependence, resulting from the finite muon lifetime, has been removed.

In Table VI, Kα X-ray results analogous to the stripping results in Table V are presented. This table gives the number of Kα X-rays emanating from an $\alpha\mu$ atom formed in a given state. Not surprisingly the most Kα X-rays come from atoms formed in the 2p state. In fact, it is important to note that on the average more than one Kα X-ray results if $\alpha\mu$ is formed in the 2p state; this excess emphasizes the importance of collisional excitation, as does the fact that a significant number of X-rays emanate even if $\alpha\mu$ is formed in its ground state. The decreasing number of Kα X-rays as $\alpha\mu$ is formed in more highly excited states is a consequence of these muons being stripped. K-series X-ray production is the best available probe of the distribution of initial $\alpha\mu$ states. Such information would be of interest as a test of the sudden approximation for sticking.

The number of Kα, Kβ, and Kγ X-rays per fusion are shown as a function of density in Fig. 14. As the density increases the number of X-rays decreases corresponding to the increasing importance of stripping and collisional de-excitation. This density dependence is greater than the density dependence predicted for ω_s and, in principle, X-ray production would go to zero in the

limit of high (unreachable, in practice) density. The higher K-series X-rays diminish the fastest as the density increases; the ratios $K\beta/K\alpha$ and $K\gamma/K\beta$ are shown in Fig. 15. Clearly the $K\beta$ and $K\gamma$ X-rays would provide useful additional information.

We next consider the sensitivity of the stripping probability R and X-ray intensity $I_{K\alpha}$ to the kinetic rates. This study is very important for understanding the kinetics as well as for future investigations since none of the collisional processes are known with great accuracy. The Stark mixing of the 2s and 2p states is of particular interest since it has not been explicitly treated before. Menshikov and Ponomarev[24] assumed that the mixing rate was infinite whereas Bracci and Fiorentini[16] took it simply to determine an effective decay rate for the n=2 level. As can be seen in Table VII neither approximation is really an adequate substitute for explicit treatment of the 2s-2p Stark mixing. It is interesting to note that the effect of the actual Stark mixing lies about midway between no mixing and complete mixing. The effect is much more important for $I_{K\alpha}$ than for R. It is least important for R at low density though the effect is not negligible even there.

Discussion of Stark mixing raises a related question; namely, how precisely do we need to know the 2s-2p branching ratios for processes which bring $\alpha\mu$ into the n=2 level? In Fig. 16 cross sections for excitation of the hydrogen atom to 2s and 2p states by proton collisions are shown.[25] The ratio $\sigma_{1,2p}/\sigma_{1,2s}$ depends strongly on velocity and is considerably greater then 3:1 at v=3 (which corresponds to v=6 for $\alpha\mu$+d collisions). This effect will be treated more precisely in the near future but, as will be shown below, it has relatively little effect on the accuracy of the present results.

The estimated uncertainties in all the rates and their effects on R and $\tau_{K\alpha}$ are given in Table VIII. It must be emphasized that the estimates of the

error bars on the rates are very subjective; they are generally not provided by the theoretical methods. The only rates that are known with certainty are the radiative rates. The stopping power for $\alpha\mu$, like a proton at the same velocity, in hydrogen is known fairly accurately; to the extent that its fit is determined by theoretical p+H calculations, the actual stopping power may be somewhat smaller because of the possibility that the $\alpha\mu$ may be neutralized to form a hydrogen-like atom during parts of its slowing down. The departure of $\sigma_{1,2p}/\sigma_{1,2s}$ from 3 is also treated at present as an uncertainty. The effects on R and $\tau_{K\alpha}$ are given for both low (ϕ=0.1) and high (ϕ=1.2) densities; in some cases the influence of a given process has an appreciable density dependence. By far the greatest uncertainty in R comes from the stripping cross section. On the other hand, the stripping cross section has relatively little influence on $\tau_{K\alpha}$, but the excitation and Stark cross sections are much more important. The overall theoretical uncertainties in R and $\tau_{K\alpha}$ are estimated to be 20-25% of their calculated values.

Actually neither R nor $\tau_{K\alpha}$ is directly obtainable by current experiments. Instead $\omega_s=(1-R)\omega_s^\circ$ and $I_{K\alpha}/\chi=\tau_{K\alpha}\omega_s^\circ$ are measured. Hence the uncertainty in the calculated value of ω_s° also must be considered. Three recent elaborate nonadiabatic calculations of ω_s° have been made.[20-22] They are in reasonably good agreement and from them I estimate

$$\omega_s^\circ = (0.88 \pm 0.05)\% \quad .$$

As before, the error bar is rather arbitrary and in this case does not include a contribution from any deficiency of the sudden approximation. In addition, it is assumed that fusion in the J=1 states, where sticking is dramatically reduced, is not important. The final theoretical extimates of R, ω_s, $\tau_{K\alpha}$, and

$I_{K\alpha}/\chi$ are given in Table IX. For the density dependence we obtain

$$\omega_s(\phi = 0.1) \; / \; \omega_s(\phi = 1.2) = 1.11 \pm 0.05$$

and

$$I_{K\alpha}(\phi = 0.1) \; / \; I_{K\alpha}\;(\phi = 1.2) = 1.23 \pm 0.08 \quad ,$$

where both error bars are due mostly to the excitation rates. It should be noted that while the stripping cross sections are very important to the magnitude of R they are not nearly so important to its density dependence. Increasing the excitation cross sections tends to increase both the magnitude and density dependence of R. The density dependence of $I_{K\alpha}$ is also somewhat sensitive to the Auger and Stark rates.

An important conclusion from the above discussion is that the measurements of neutron and X-ray yields should be regarded as <u>complementary</u> rather than as alternatives. A third diagnostic exists that may be accessible in d-t MCF experiments, namely, detection of the charged species α and $\alpha\mu$.[v] Charged-particle detection would provide the most direct measurement of sticking. Comparison with all the experimental observables provides a very rigorous test of the theoretical treatment of $\alpha\mu$ kinetics.

The present calculation of ω_s is compared with other theoretical[16,24,26,27] and experimental[1b,2b,28] values in Table X. At high density the agreement with the experimental determinations is reasonably good. It is remarkable that the sticking is a factor of 2 smaller than the value accepted for many years. At low density the disagreement between experiments has to be

---

[v]Such an experiment has been proposed at LAMPF.

resolved before conclusive comparison is possible. Finally the present determination of $I_{K\alpha}$ is compared with other theoretical[16,27] and experimental[29] values in Table XI. The agreement of the present calculation with experiment is excellent.

ACKNOWLEDGMENTS

I am indebted to Mel Leon for numerous stimulating discussions. This work was supported by the U.S. Department of Energy, in large part by the Division of Advanced Energy Projects.

REFERENCES

1. (a) S. E. Jones et al., Phys. Rev. Lett. 51 (1983) 1757;
   (b) 56 (1986) 588.

2. (a) W. H. Breunlich et al., Phys. Rev. Lett. 53 (1984) 1137;
   (b) Phys. Rev. Lett. xx (1986) xxxx.

3. J. S. Cohen and M. Leon, Phys. Rev. Lett. 55 (1985) 52.

4. P. Kammel, Lett. Nuovo Cimento 43 (1985) 349.

5. M. Leon, Phys. Rev. Lett. 52 (1984) 605.

6. M. Leon, Proc. of the International Symposium on Muon-Catalyzed Fusion μCF-86, and references therein.

7. J. S. Cohen and M. Leon, Phys. Rev. A 33 (1986) 1437.

8. J. S. Cohen, Phys. Rev. A 27 (1983) 167.

9. L. I. Menshikov and L. I. Ponomarev, Z. Phys. D 2 (1986) 1.

10. S. S. Gershtein, Zh. Eksp. Teor. Fiz. 34 (1958) 463 [Sov. Phys. - JETP 7 (1958) 318].

11. J. S. Cohen, Phys. Rev. A 34 (1986) xxxx.

12. R. G. Sachs and E. Teller, Phys. Rev. 60 (1941) 18.

13. A. Adamczak, V. S. Meleshik, and L. I. Menshikov, I. V. Kurchatov Institute of Atomic Energy preprint E4-86-29 (1986).

14. J. S. Cohen, Phys. Rev. A 26 (1982) 3008, and references therein.

15. J. S. Cohen and G. Fiorentini, Phys. Rev. A 33 (1986) 1590.

16. L. Bracci and G. Fiorentini, Nucl. Phys. A364 (1981) 383.

17. H. A. Bethe and E. Salpeter, Quantum Mechanics of One- and Two-Electron Atoms (Academic Press, New York, 1957).

18. M. Leon and H. A. Bethe, Phys. Rev. 127 (1962) 636.

19. H. H. Andersen and J. F. Ziegler, Hydrogen Stopping Powers and Ranges in All Elements (Pergamon Press, New York, 1977).

20. C.-Y. Hu, Phys. Rev. A 34 (1986) 2536.

21. D. Ceperley and B. J. Alder, Phys. Rev. A 31 (1985) 1999.

22. L. N. Bogdanova et al., Nucl. Phys. A454 (1986) 653.

23. V. E. Markushin, Abstracts of the Tenth International Conference on Atomic Physics, Tokyo, 1986, ed. H. Narumi and I. Shimamura, p. 116.

24. L. I. Menshikov and L. I. Ponomarev, Pis'ma Zh. Eksp. Teor. Fiz. 41 (1985) 511 [JETP Lett. 41 (1985) 623].

25. D. R. Bates and G. Griffing, Proc. Phys. Soc. A 66 (1953) 961.

26. S. S. Gershtein et al., Zh. Eksp. Teor. Fiz. 80 (1981) 1690 [Sov. Phys. - JETP 53 (1981) 872].

27. H. Takahashi, Fusion Technology 9 (1986) 328; Phys. Lett. B 174 (1986) 133.

28. W. H. Breunlich et al., Proc. of the International Symposium on Muon-Catalyzed Fusion μCF-86.

29. H. Bossy et al., Proc. of the International Symposium on Muon-Catalyzed Fusion μCF-86.

TABLE I

$dt\mu$ FORMATION: AVERAGE VALUES

(a)

Average time of molecular formation $\bar{t}_{mf}$ (normalized to ϕ=1)*

T(K)	c_t		
	0.1	0.5	0.9
30	1.87 ns	5.9 ns	112 ns
300	2.05 ns	5.8 ns	70 ns

*Using molecular formation rates from Jones et al. (1986).

(b)

Effective temperature $[E_{av}/(1.5\ k)]$ at average time of molecular formation

T(K)	c_t		
	0.1	0.5	0.9
30	172 K	108 K	31 K
300	345 K	334 K	300 K

TABLE II

$dt\mu$ FORMATION: TRANSIENTS

"Epithermal time"--arbitrarily defined as time at which $E_{av}/(1.5\ k)$ falls below 600 K (normalized to ϕ=1).

T(K)	c_t		
	0.1	0.5	0.9
30	0.5 ns	0.9 ns	3.1 ns
300	0.6 ns	1.1 ns	3.9 ns

TABLE III

DEPENDENCE OF σ_n^{st} ON ELECTRONIC STRUCTURE

	Target	σ_1^{st}	σ_2^{st}	σ_3^{st}
v = 1 a.u.	d	0.96	17.4	51.3
	D_{eff}	0.96	17.6	51.1
	de	0.90	17.4	51.2
v = 6 a.u.	d	0.145	0.60	1.30
	D_{eff}	0.145	0.60	1.30
	de	0.146	0.59	1.33

TABLE IV

DEPENDENCE OF σ_n^{st} ON TARGET MASS

Target	σ_1^{st} (v=2)	σ_1^{st} (v=6)
p	1.07	0.145
d	1.11	0.145
t	1.14	0.144

TABLE V

DEPENDENCE OF STRIPPING ON INITIAL STATE OF $\alpha\mu$

$\phi = 1$

State	Initial $\alpha\mu$ distribution	Fraction stripped	Contribution to R
1s	0.7731	0.339	0.262
2s	0.1106	0.498	0.055
2p	0.0269	0.361	0.010
n=3	0.0434	0.620	0.027
n=4	0.0186	0.787	0.015
n=5	0.0090	0.842	0.008
n=6	0.0052	0.865	0.004
n=7	0.0033	0.875	0.003
n=8	0.0022	0.880	0.002
n≥9	0.0077	~0.9	0.007
Total	1.0000		0.393

TABLE VI

DEPENDENCE OF Kα X-RAYS ON INITIAL STATE OF αμ

$\phi = 1$

State	Initial αμ distribution	Kα X-rays per αμ formed in this state	Contribution to $I_{K\alpha}/\chi$ (X 100)
1s	0.7731	0.172	0.117
2s	0.1106	0.750	0.073
2p	0.0269	1.112	0.026
n=3	0.0434	0.347	0.013
n=4	0.0186	0.183	0.0030
n=5	0.0090	0.134	0.0011
n=6	0.0052	0.114	0.0005
n=7	0.0033	0.105	0.0003
n=8	0.0022	0.101	0.0002
n≥9	0.0077	~0.09	0.0006
Total	1.0000		0.235

TABLE VII

SENSITIVITY TO STARK MIXING RATES

Stark factor	R		$\frac{100}{\chi} I_{K\alpha}$	
	ϕ=1.2	ϕ=0.1	ϕ=1.2	ϕ=0.1
0	0.44	0.35	0.15	0.20
0.1	0.43	0.35	0.17	0.22
0.5	0.41	0.34	0.21	0.26
1	0.40	0.33	0.23	0.28
2	0.39	0.32	0.25	0.30
10	0.38	0.32	0.27	0.32
∞	0.37	0.32	0.28	0.33
BF*	0.43	0.32	0.18	0.32

*Bracci & Fiorentini (1981) treatment of Stark mixing as effective decay rate of the n=2 level:

$$\Lambda^{2\to 1} = \Lambda^{(2s\to 2p)}_{\text{Stark}} + \Lambda^{(2\to 1)}_{\text{rad}} - \left[\left(\Lambda^{(1s\to 2p)}_{\text{Stark}}\right)^2 + \left(\Lambda^{(2\to 1)}_{\text{rad}}\right)^2\right]^{\frac{1}{2}}$$

Observe that this treatment of the n=2 level yields a stronger density dependence, especially in $I_{K\alpha}$.

TABLE VIII

ESTIMATED UNCERTAINTIES DUE TO RATES

Process & Uncertainty		ϕ	Effect on R ($\Delta R/R$)	Effect on $\gamma_{K\alpha}$
Stripping (ion.+trans.)	±30%	1.2	±18%	∓6%
		0.1	±23%	∓4%
Excitation (& deexcit.)	±40%	1.2	±8%	±15%
		0.1	±3%	±20%
Auger	×÷2	1.2	∓4%	±4%
		0.1	∓2%	±2%
Radiation	0	1.2	0	0
		0.1	0	0
Stark	×÷3	1.2	∓4%	±13%
		0.1	∓3%	±10%
Stopping power	±10%	1.2	∓7%	∓6%
		0.1	∓8%	∓6%
σ_{2p}/σ_{2s}	x4 +2	1.2	∓1%	±3%
		0.1	∓1%	±3%
Total uncertainty		1.2	±22%	±22%
		0.1	±25%	±24%

TABLE IX

PRESENT BEST ESTIMATES

ϕ	R(%)	ω_s(%)	$\gamma_{K\alpha}$	$(I_{K\alpha}/\chi)X100$
0.1	33±8	0.59±0.08	0.32±0.08	0.28±0.07
1.2	40±9	0.53±0.09	0.26±0.06	0.23±0.05

TABLE X

COMPARISON WITH OTHER DETERMINATIONS OF ω_s

	$\omega_s(\%)^*$	
	$\phi = 1.2$	$\phi = 0.1$
Present	0.53 ± 0.09	0.59 ± 0.08
Menshikov & Ponomarev (1985)	0.60	0.67
Takahashi (1986)	0.61 - 0.67	0.62 - 0.69
Bracci & Fiorentini (1981)	0.67	0.70
Gershtein et al. (1981)	0.68	
Jones et al. (expt. 1986)	0.35 ± 0.07	1.1 ± 0.4
Breunlich et al. (expt. 1986)	0.45 ± 0.05	0.50 ± 0.1

*Important: Note that all theoretical values are obtained by $\omega_s = (1\text{-}R)\,\omega_s^\circ$ with $\omega_s^\circ = 0.88\%$ and R as given by that theory.

TABLE XI

COMPARISON WITH OTHER DETERMINATIONS OF $I_{K\alpha}$

	$I_{K\alpha}/\chi(\%)^*$	
	$\phi = 1.2$	$\phi = 0.1$
Present	0.23 ± 0.05	0.28 ± 0.07
Takahashi (1986)	0.36	0.35
Bracci & Fiorentini (1981)	~0.40†	
Bossy et al. (expt. 1986)	0.25 ± 0.05	

*Note that all theoretical values are obtained assuming $\omega_s^\circ = 0.88\%$.

†Estimated since only $I_{K(total)}$ was given by Bracci & Fiorentini.

Figure Captions

1. Cross sections for $t\mu+d$ and $t\mu+t$ elastic scattering and $t\mu+t$ hyperfine transitions.

2. Monte Carlo histogram and its fit at time 2 μs after $t\mu$ formation in a target with c_t=0.5 and T=300 K.

3. Kinetic-energy distributions of $t\mu$ at several times in a target with c_t=0.5 and T=30 K.

4. Average energy distributions of $t\mu$ as a function of time for targets with c_t = 0.1, 0.5, and 0.9 at temperatures 30 and 300 K.

5. Fraction of $t\mu$ atoms in the triplet hyperfine state as a function of time for targets with c_t = 0.1, 0.5, and 0.9.

6. Schematic of $\alpha\mu$ kinetics.

7. Stripping and excitation rates for $\alpha\mu$ in the n=1 level and the kinetic energy loss ($\Delta E/E$) rate for all states in a target with density ϕ=1.

8. Rates out of the n = 2 level of $\alpha\mu$ at density ϕ=1.

9. Rates out of the n = 3 level of $\alpha\mu$ at density ϕ=1.

10. Rates out of the n = 6 level of $\alpha\mu$ at density ϕ=1.

11. Time-dependent state populations, stripping fraction, and surviving fraction of the initial kinetic energy for $\alpha\mu$ in a target with density ϕ=1. This calculation takes $\sigma_{1,2p}/\sigma_{1,2s}$=3.

12. Stripping fraction and sticking percentage obtained with different numbers of $\alpha\mu$ states, n_{max} = 1 to 10. The density is ϕ=1.

13. Stripping fraction and sticking percentage as a function of density.

14. Numbers of Kα, Kβ, and Kγ $\alpha\mu$ X-rays per fusion as a function of density.

15. Ratios of Kβ/Kα and Kγ/Kα $\alpha\mu$ X-ray intensities as a function of density.

16. Cross sections for excitation of the 2s and 2p states of H in proton collisions with the ground-state hydrogen atom (from Ref. 25).

FIG. 1

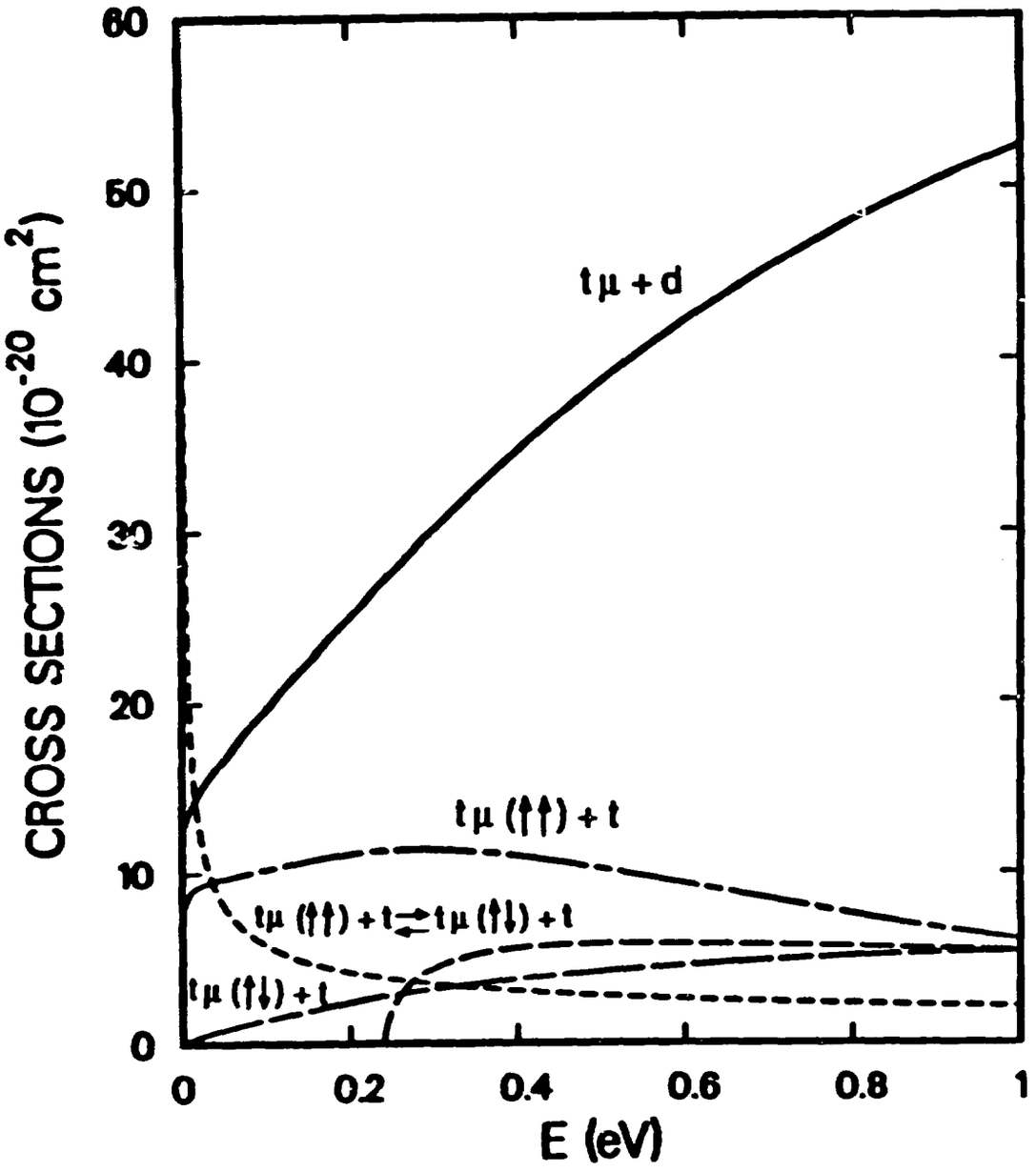
CROSS SECTIONS (10^{-20} cm^2)
60
50
40
30
20
10
0
0
0.2
0.4
0.6
0.8
1
E (eV)
tμ + d
tμ (↑↑) + t
tμ (↑↑) + t ⇌ tμ (↑↓) + t
tμ (↑↓) + t

FIG. 2

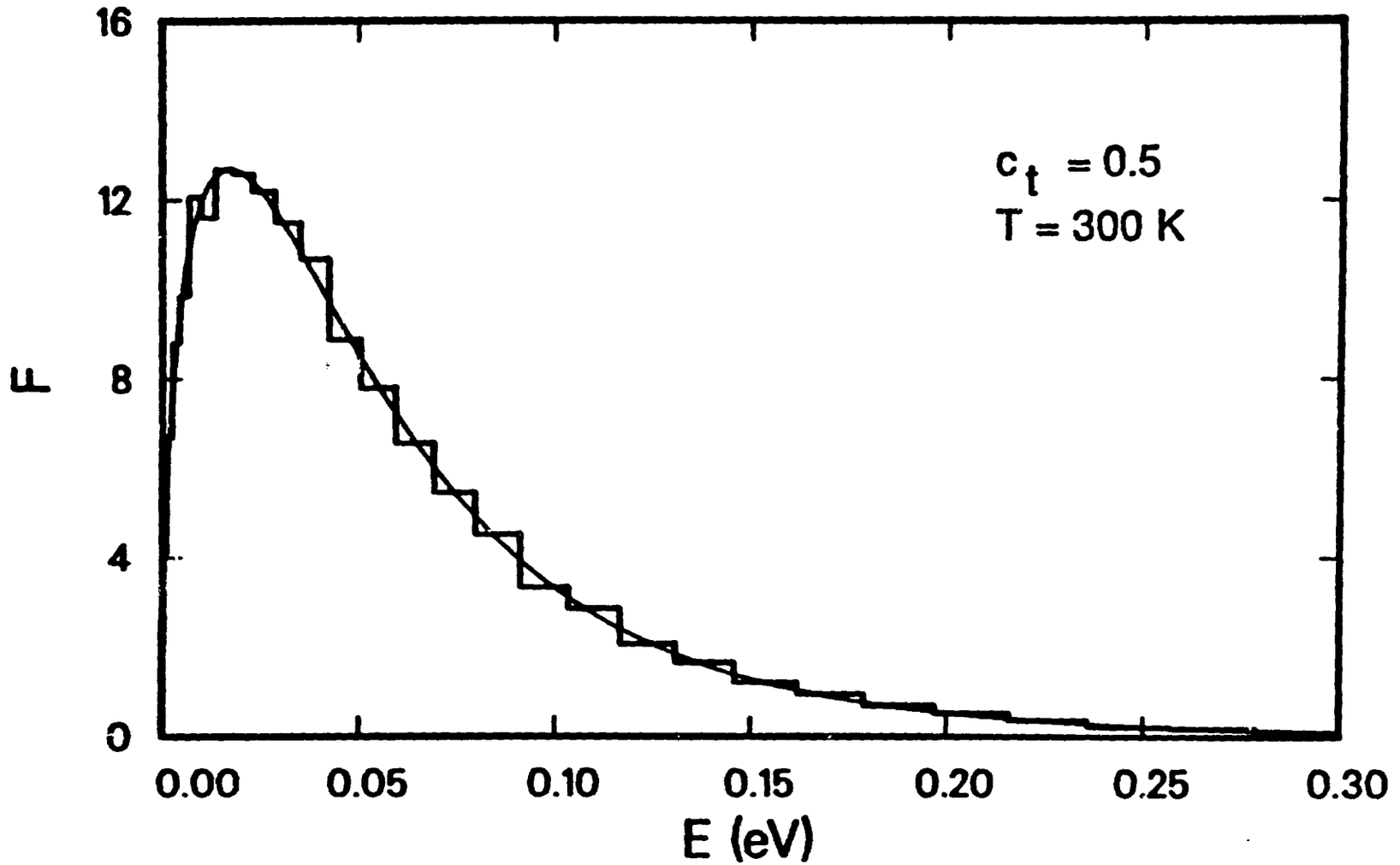

FIG. 3

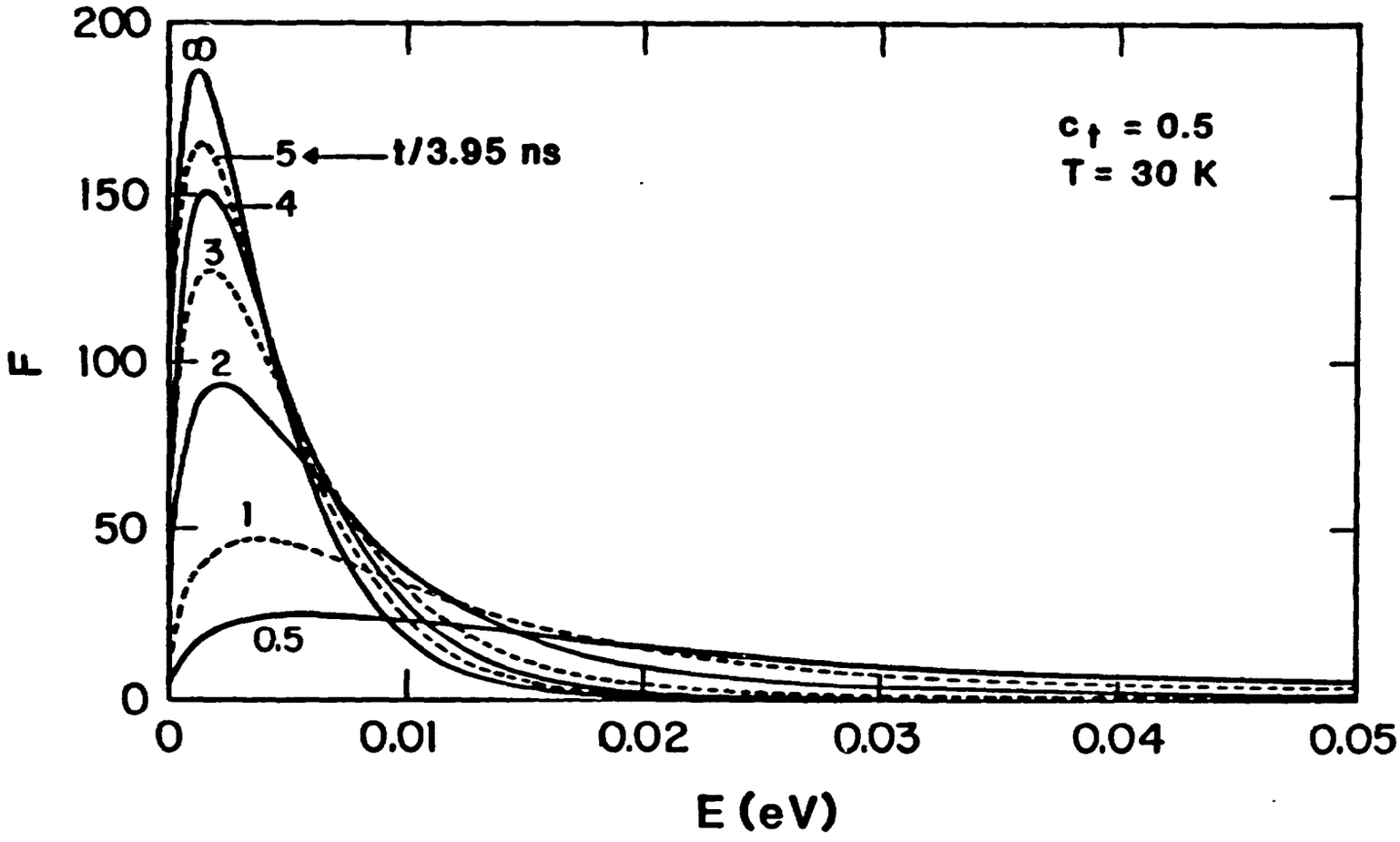
200
150
100
50
0
F
∞
5
t/3.95 ns
4
3
2
1
0.5
c_f = 0.5
T = 30 K
0
0.01
0.02
0.03
0.04
0.05
E (eV)

FIG. 4

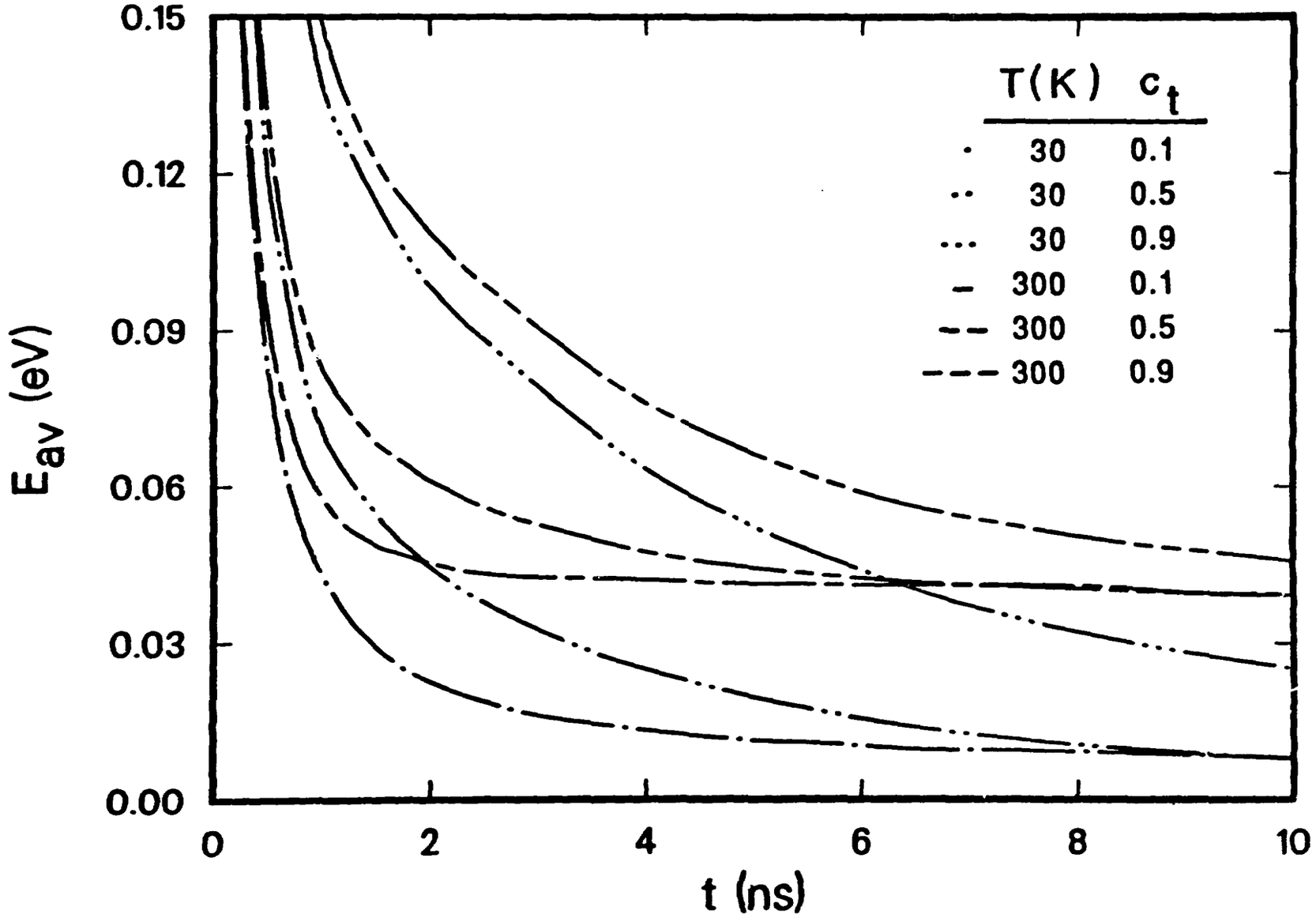
0.15
0.12
0.09
0.06
0.03
0.00
E_{av} (eV)
0
2
4
6
8
10
t (ns)
T(K) c_t
30 0.1
30 0.5
30 0.9
300 0.1
300 0.5
300 0.9

FIG. 5

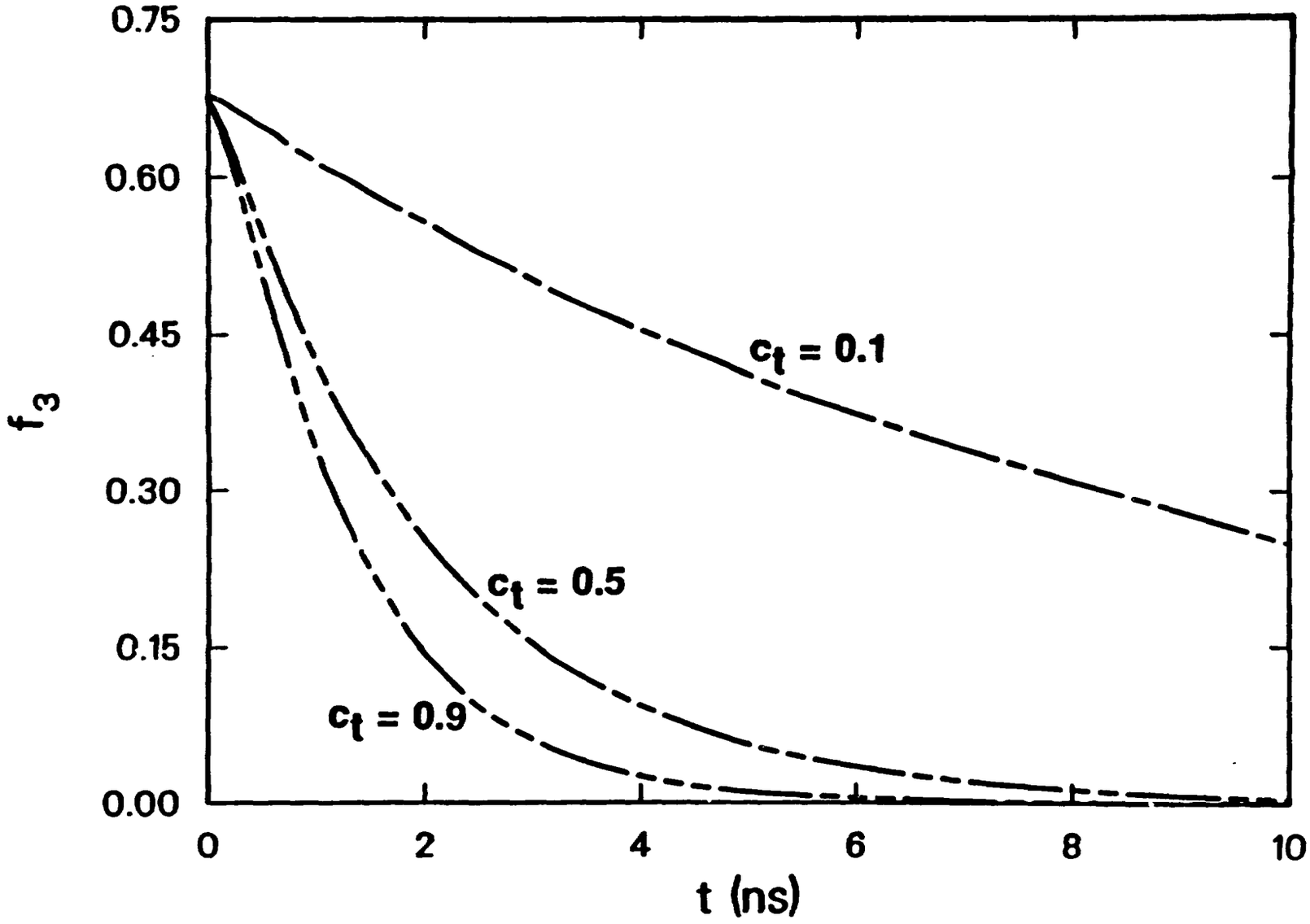

FIG. 6

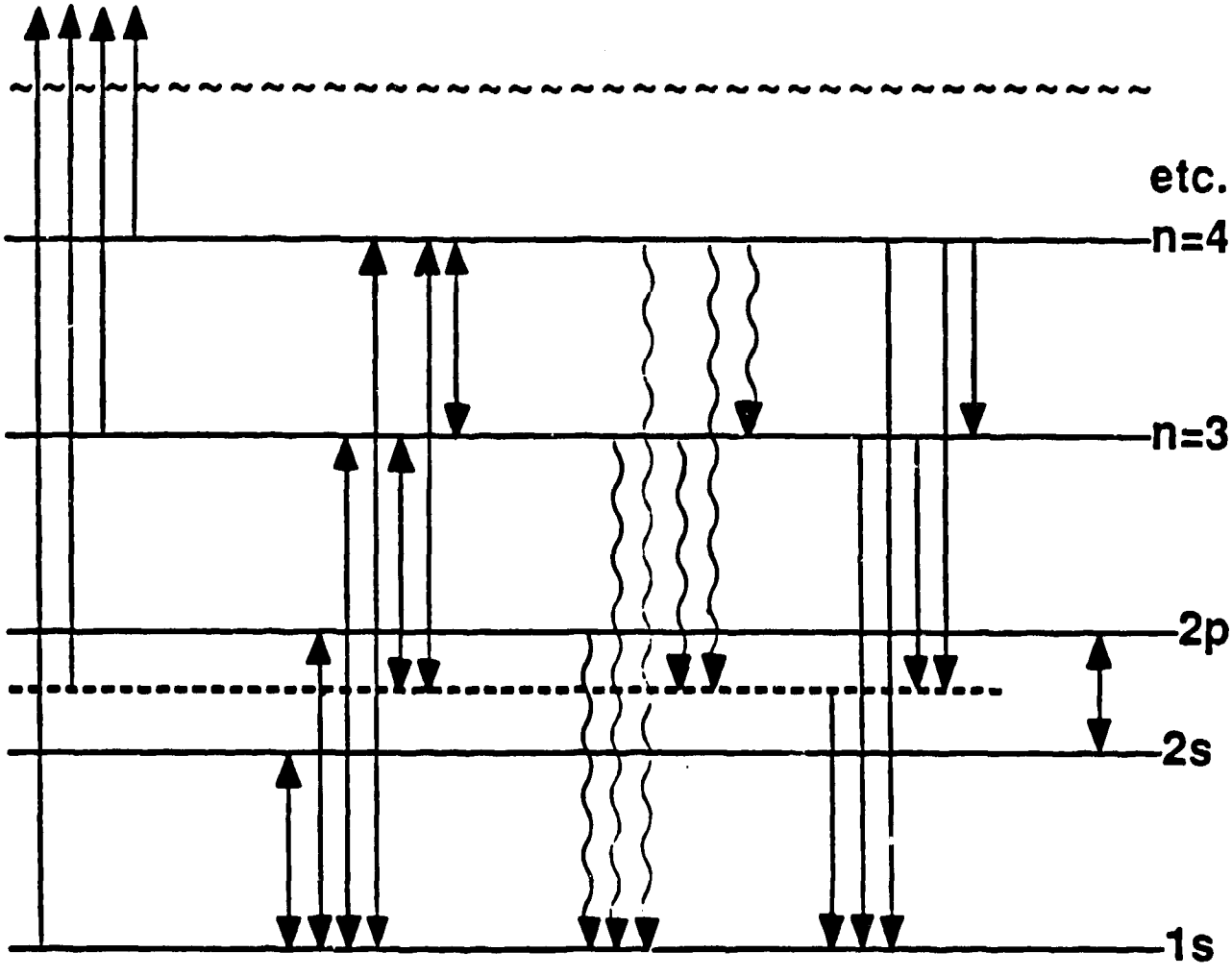

Stripping (ionization or charge transfer)

Inelastic excitation and de-excitation

Radiation

Auger

Stark

FIG. 7

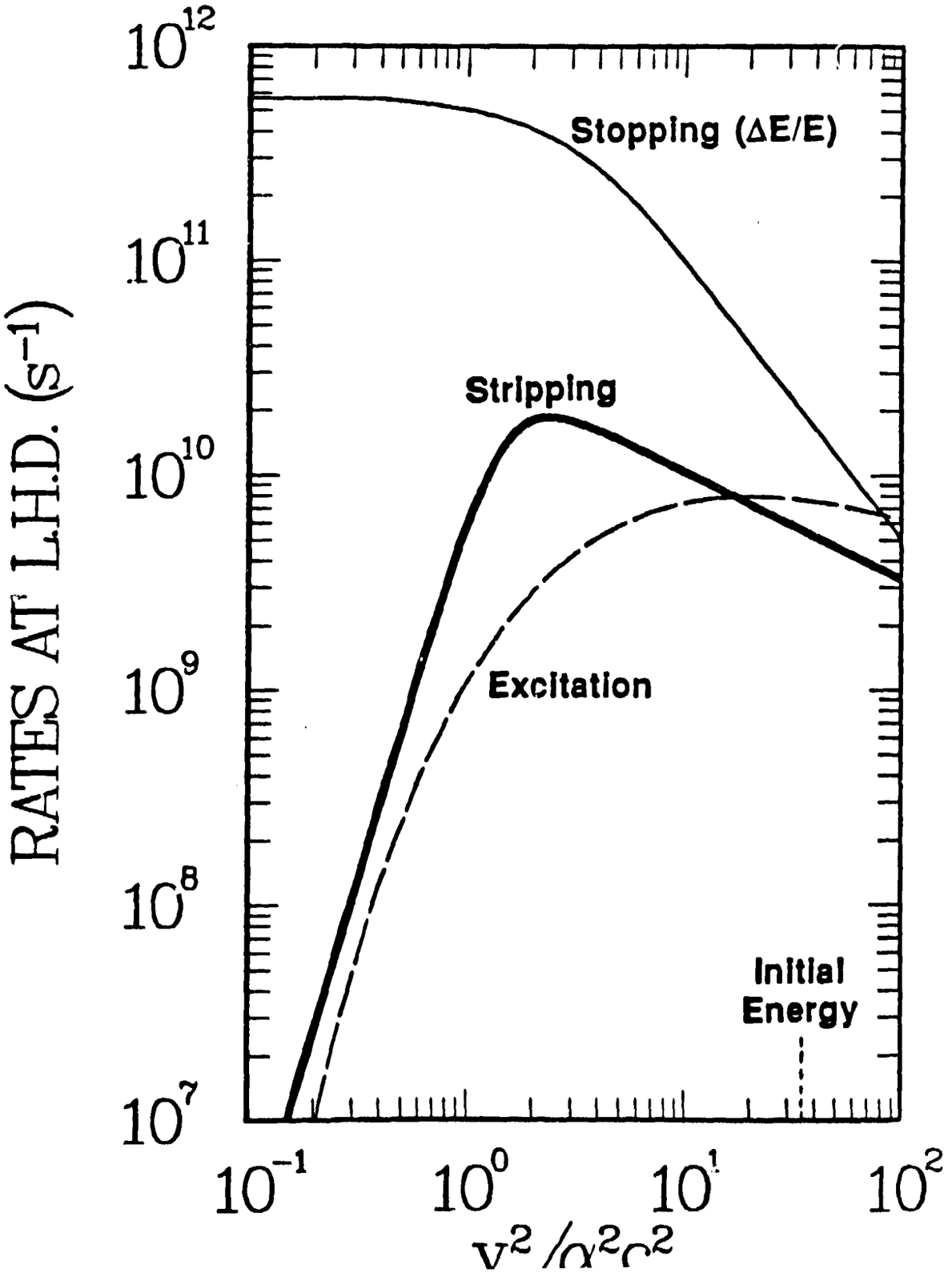
RATES AT L.H.D. (s^{-1})
10^{12}
10^{11}
10^{10}
10^{9}
10^{8}
10^{7}
Stopping (ΔE/E)
Stripping
Excitation
Initial Energy
10^{-1}
10^{0}
10^{1}
10^{2}
v^2/α^2c^2

FIG. 8

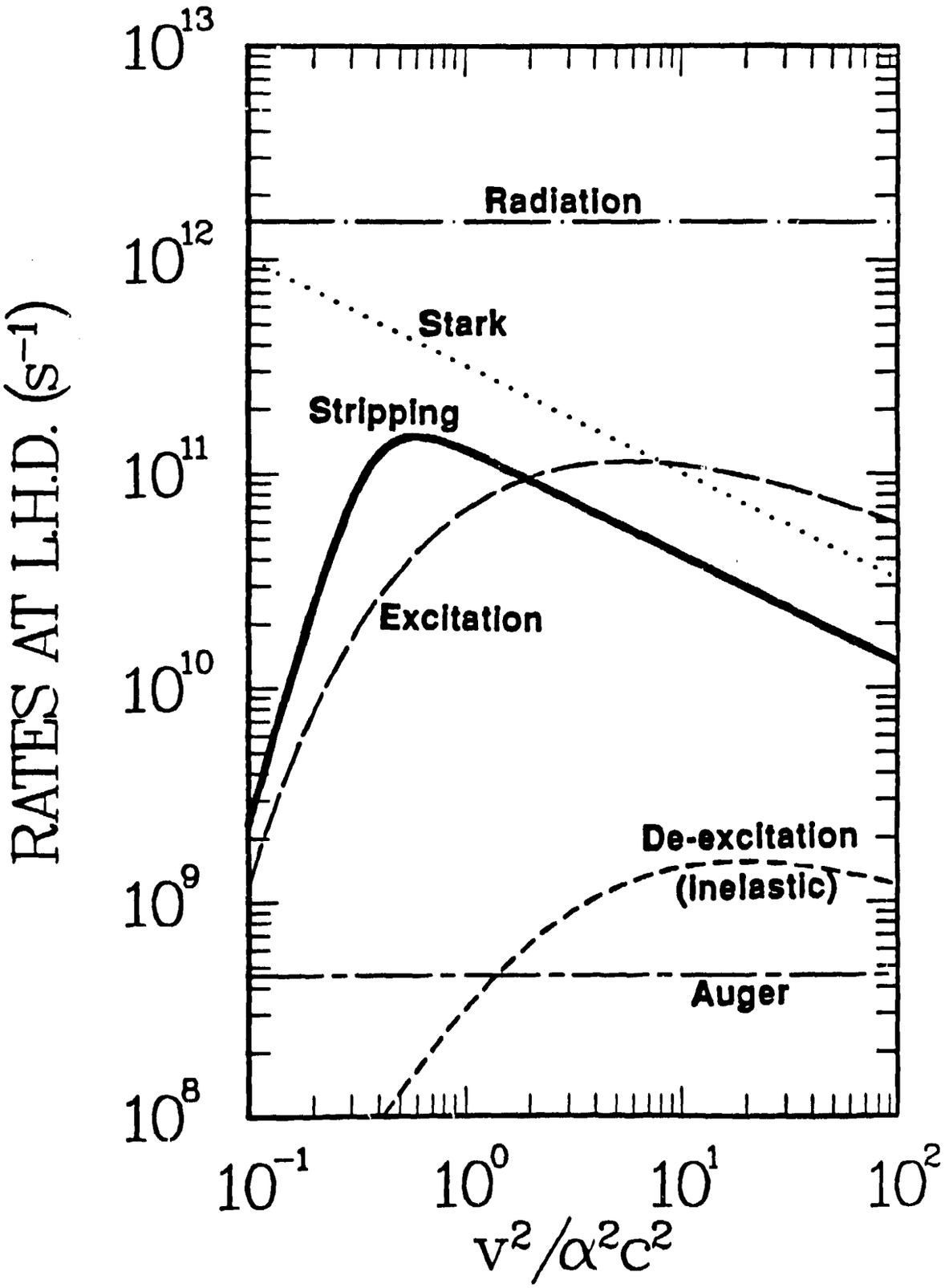
RATES AT L.H.D. (s^{-1})
10^{13}
10^{12}
10^{11}
10^{10}
10^{9}
10^{8}
Radiation
Stark
Stripping
Excitation
De-excitation
(inelastic)
Auger
10^{-1}
10^{0}
10^{1}
10^{2}
v^2/α^2c^2

FIG. 9

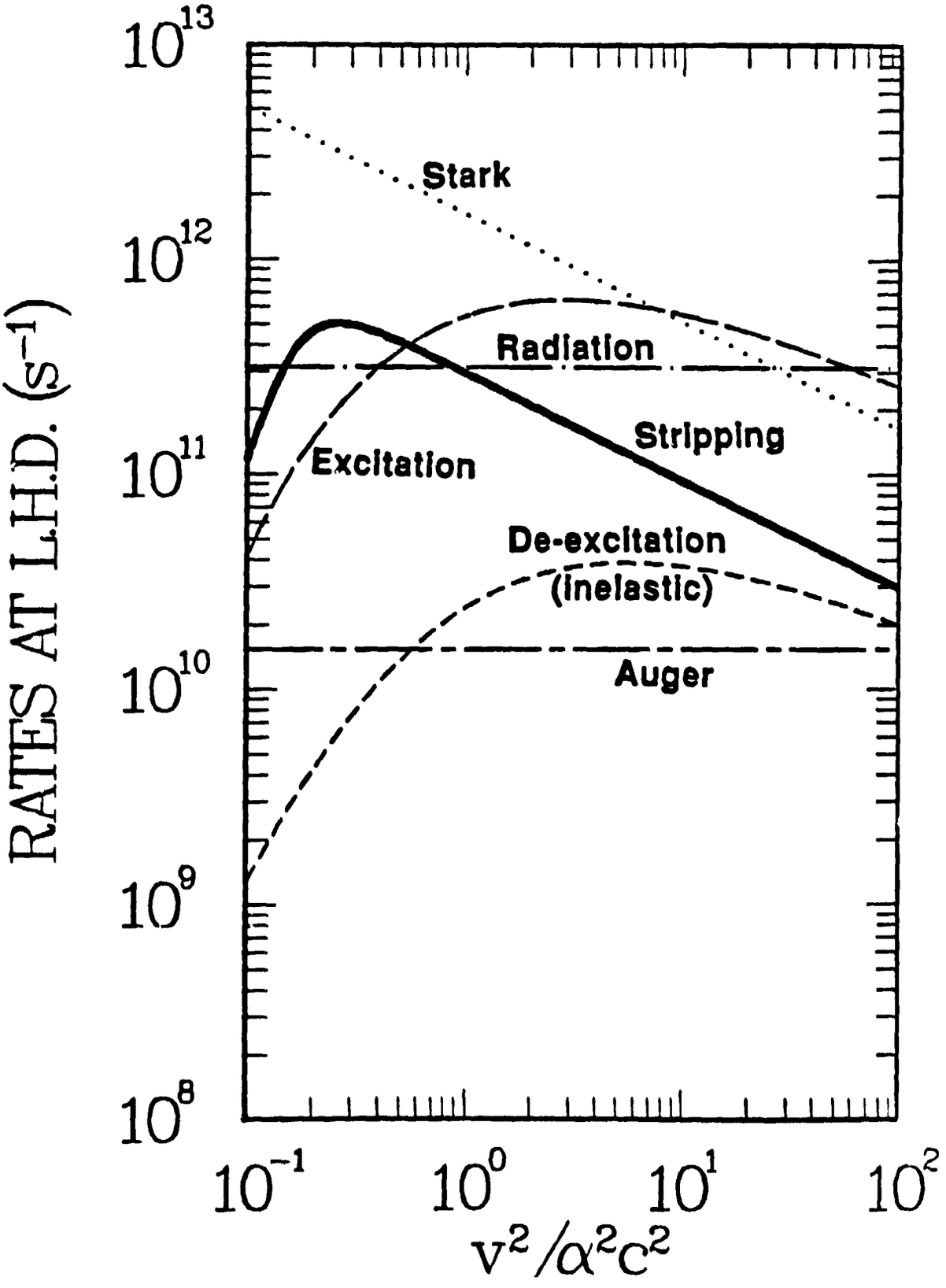
RATES AT L.H.D. (s^{-1})
10^{13}
10^{12}
10^{11}
10^{10}
10^{9}
10^{8}
Stark
Radiation
Stripping
Excitation
De-excitation
(inelastic)
Auger
10^{-1}
10^{0}
10^{1}
10^{2}
v^2/α^2c^2

FIG. 10

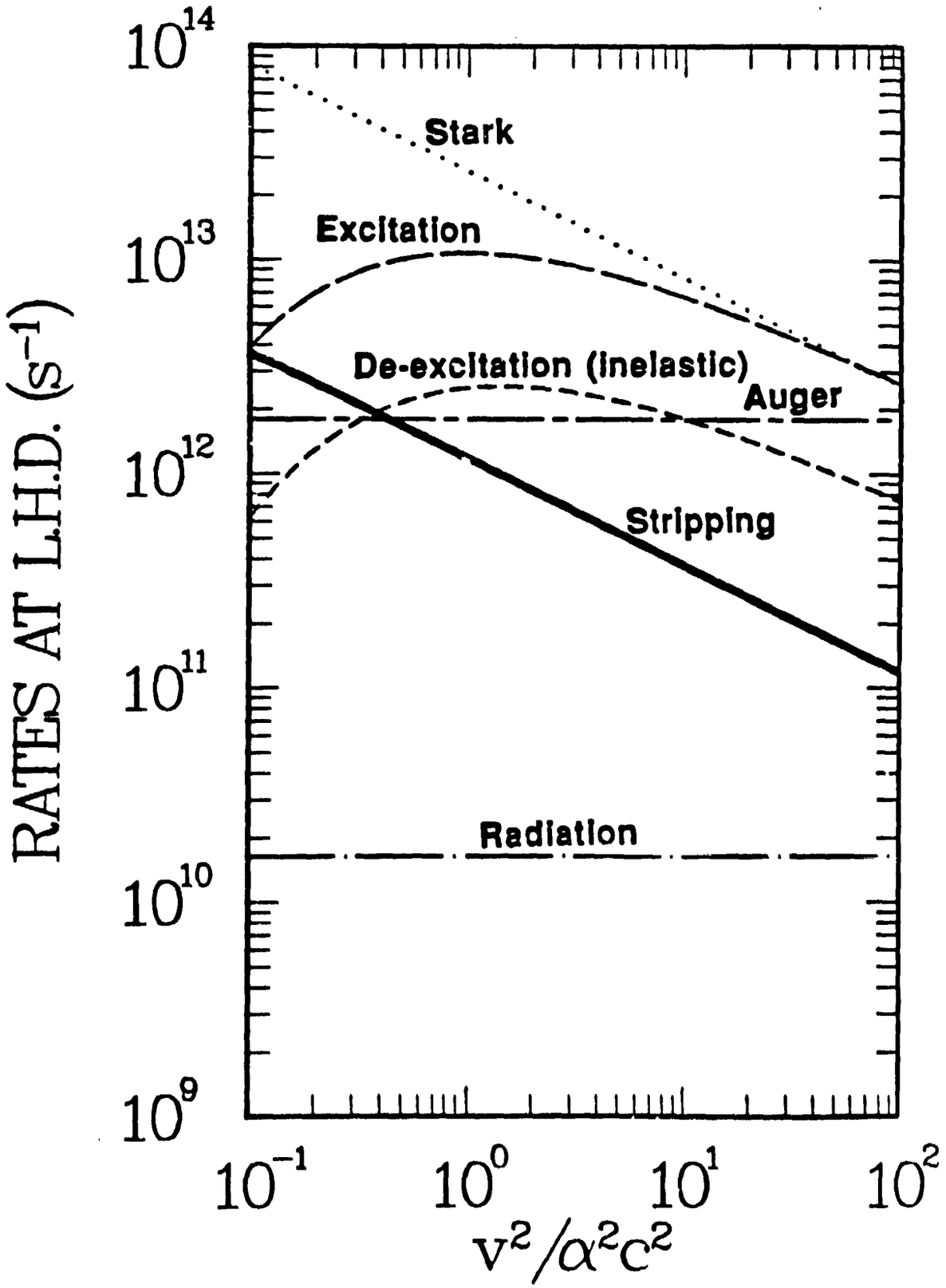
RATES AT L.H.D. (s^{-1})
10^{14}
10^{13}
10^{12}
10^{11}
10^{10}
10^{9}
Stark
Excitation
De-excitation (inelastic)
Auger
Stripping
Radiation
10^{-1}
10^{0}
10^{1}
10^{2}
v^2/α^2c^2

FIG. 11

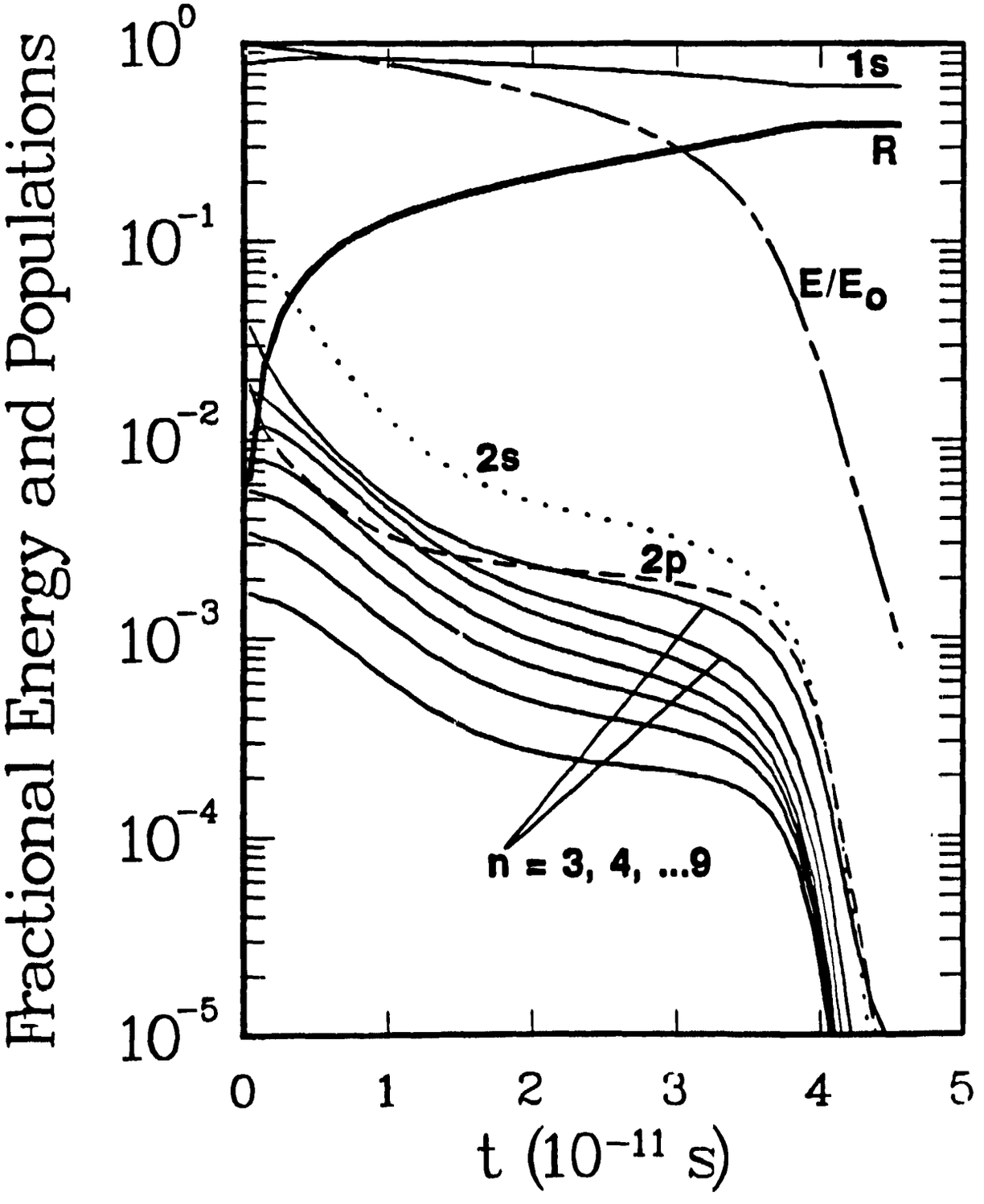
Fractional Energy and Populations
10^0
10^{-1}
10^{-2}
10^{-3}
10^{-4}
10^{-5}
1s
R
E/E_o
2s
2p
n = 3, 4, ...9
0
1
2
3
4
5
t (10^{-11} s)

FIG. 12

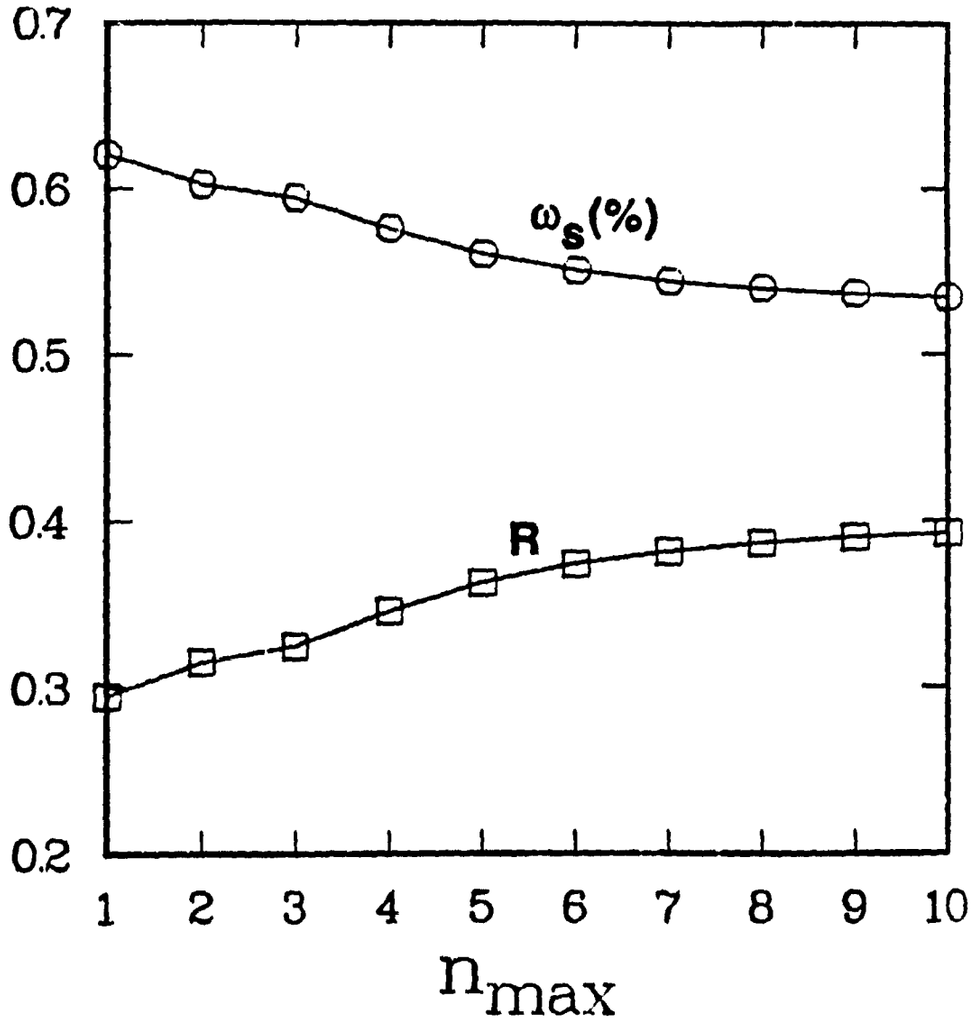

FIG. 13

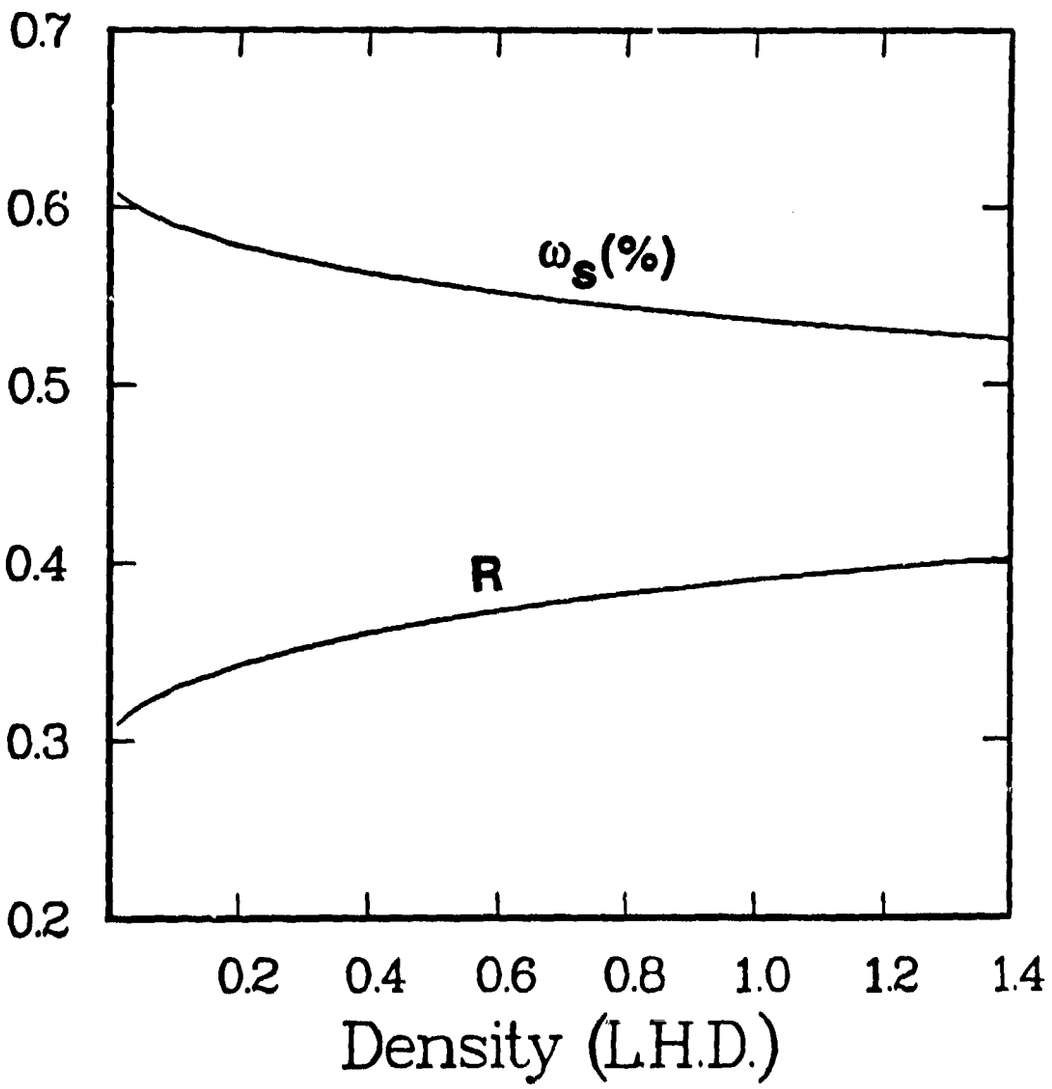

FIG. 14

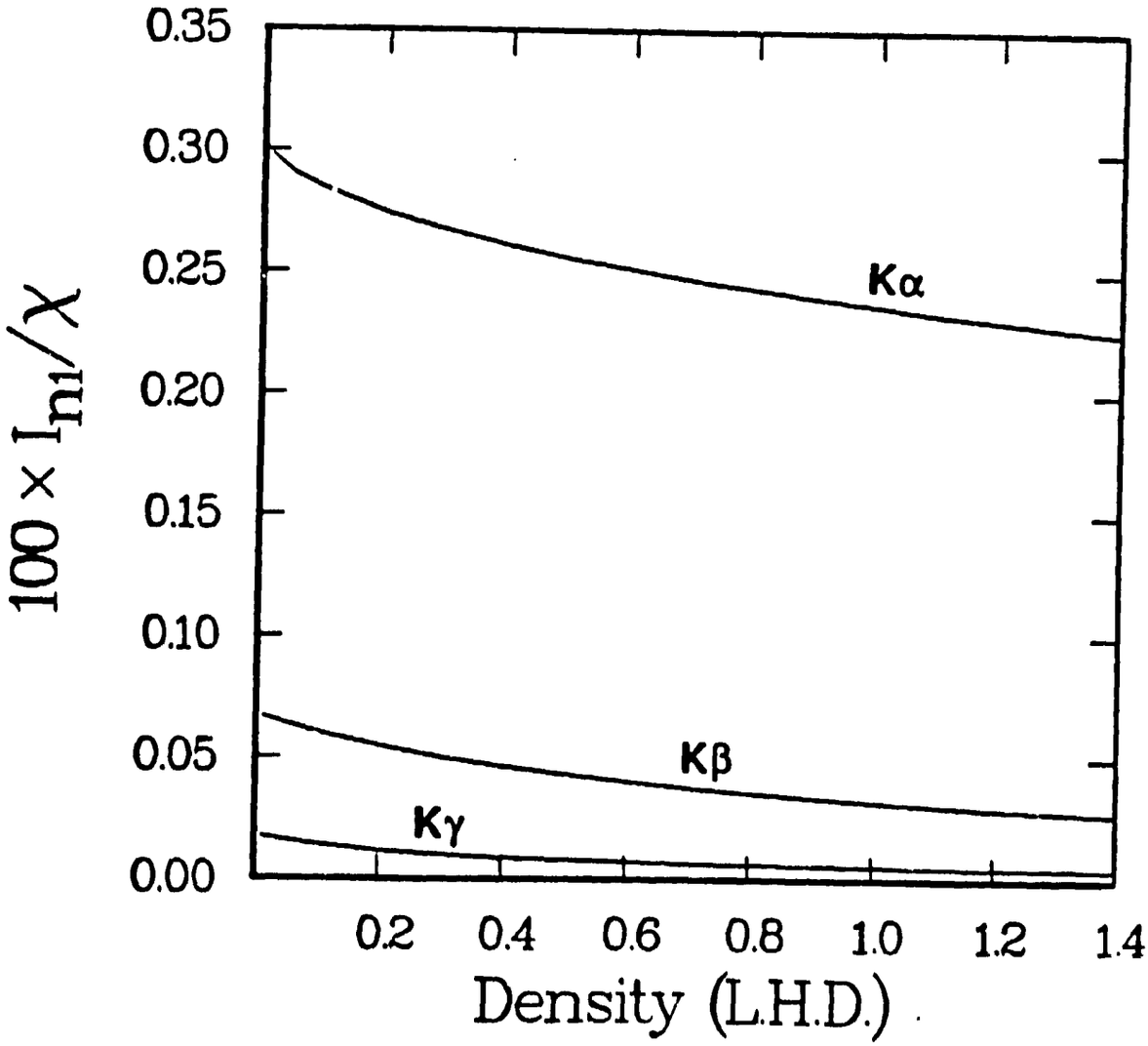
0.35
0.30
0.25
0.20
0.15
0.10
0.05
0.00
100 × I_n1/χ
Kα
Kβ
Kγ
0.2
0.4
0.6
0.8
1.0
1.2
1.4
Density (L.H.D.)

FIG. 15

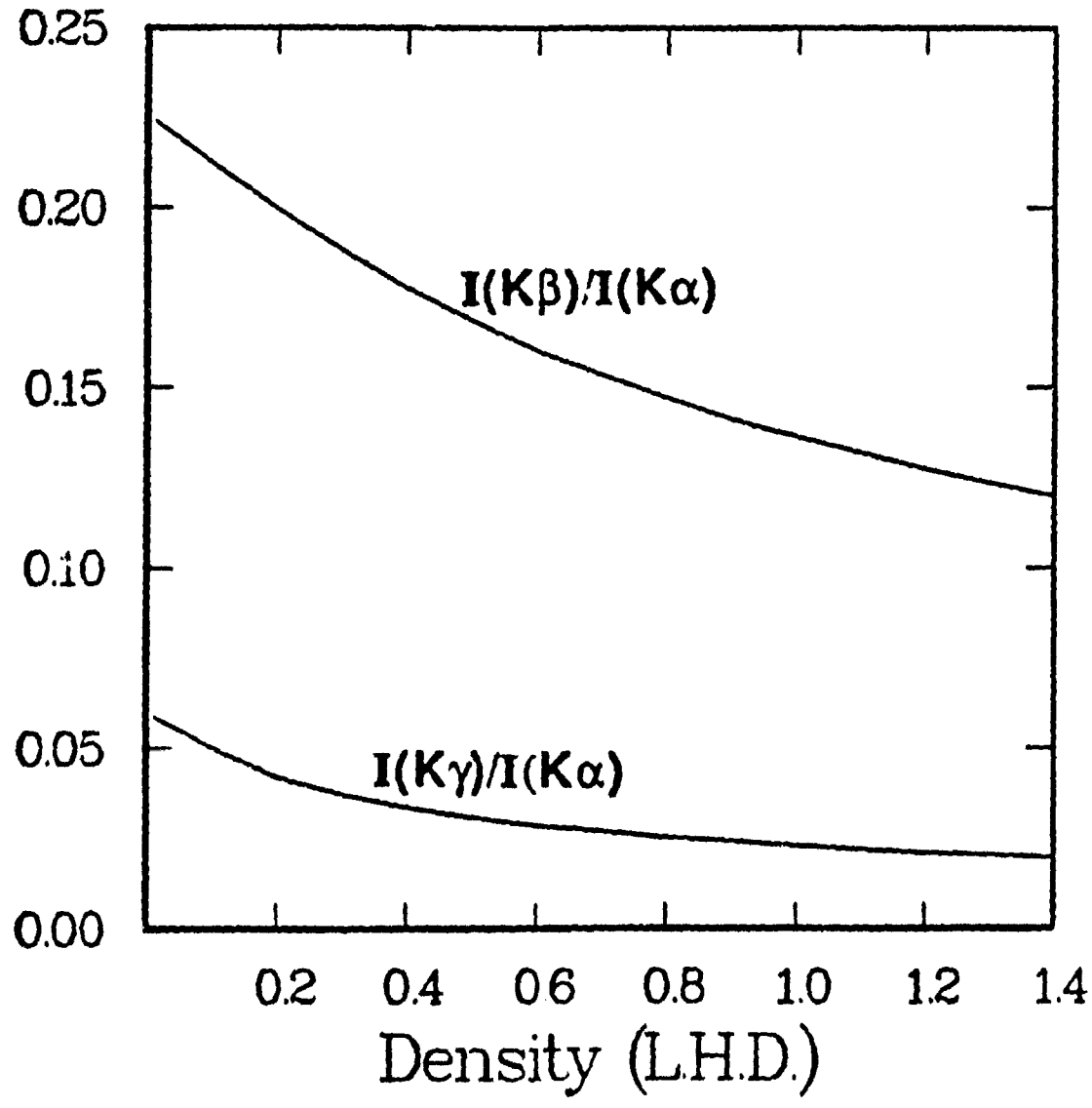
0.25
0.20
0.15
0.10
0.05
0.00
I(Kβ)/I(Kα)
I(Kγ)/I(Kα)
0.2
0.4
0.6
0.8
1.0
1.2
1.4
Density (L.H.D.)

FIG. 16

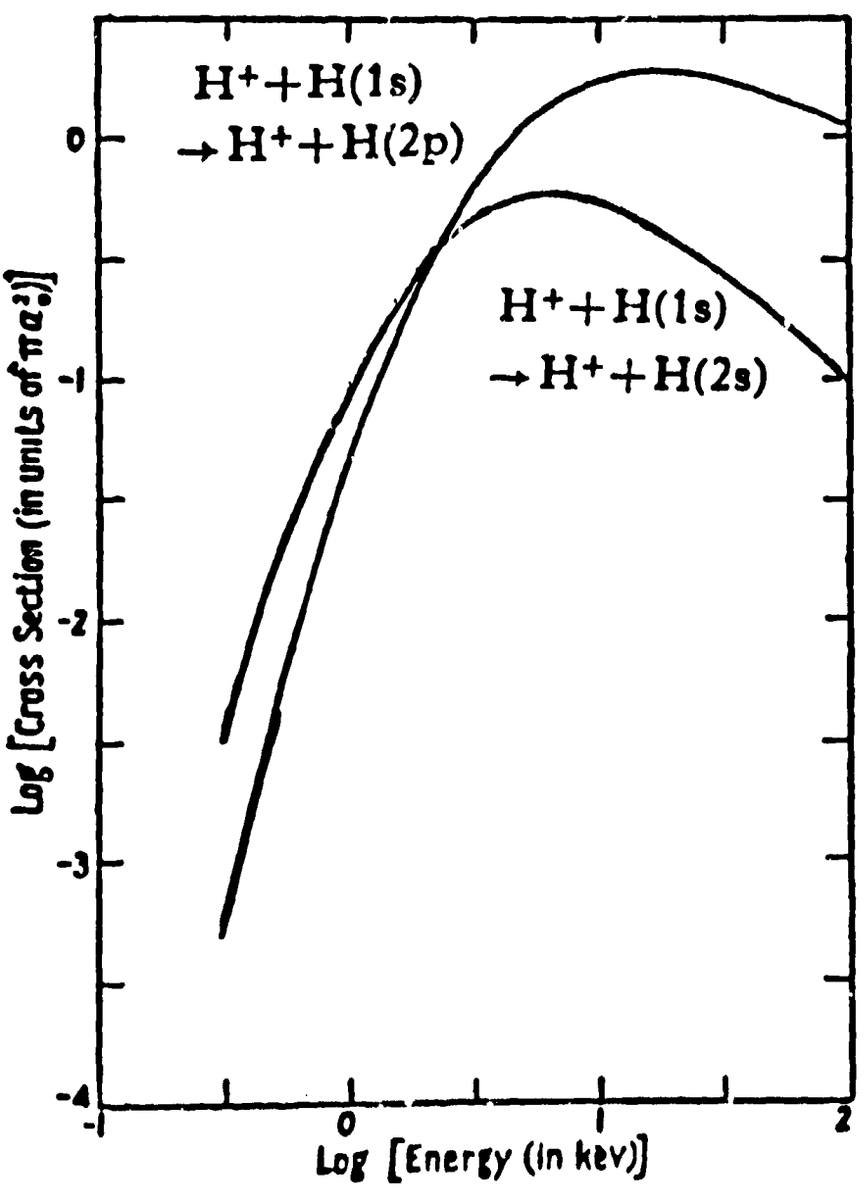
H⁺+H(1s)
→H⁺+H(2p)
H⁺+H(1s)
→H⁺+H(2s)
Log [Cross Section (in units of πa₀²)]
0
-1
-2
-3
-4
-1
0
1
2
Log [Energy (in kev)]